Accuracy and Uncertainty Assessment of Spatial Interpolation Methods for Reservoir Bathymetric Modelling

Khasanov, K.,[1]* Bakiev, M.,[1] Djabbarova, S.,[1] Norboeva, D.,[2,3] Vafoeva, O.,[1] Rakhmatilloyeva, K.[4] and Mulladjanova, G.[4]

[1]"Tashkent Institute of Irrigation and Agricultural Mechanization Engineers" National Research University, Tashkent, Uzbekistan

[2]University of Geological Sciences, Tashkent, Uzbekistan

[3]Alfraganus University, Tashkent, Uzbekistan

[4]Samarkand State Architecture and Construction University Named after Mirzo Ulugbek, Uzbekistan

Corresponding Author: kh.khasanov@outlook.com

DOI: https://doi.org/10.52939/ijg.v22i10.5237

Abstract

Accurate estimates of reservoir storage and long-term capacity loss are essential for reliable operation, sediment-management planning, and risk-informed decision making. However, bathymetric point surveys are irregularly distributed, and the reconstruction of the submerged surface introduces interpolation uncertainty that propagates into stage–storage curves and capacity-loss estimates. This study investigates the influence of spatial interpolation uncertainty on reservoir capacity-loss estimates and evaluates long-term sedimentation by comparing reservoir-bed conditions in 1987 and 2023 using Kamashi Reservoir (Uzbekistan) as a case study. Historical reservoir-bed conditions were reconstructed from digitized and georeferenced engineering topographic maps prepared in 1987, while the 2023 reservoir bed was modelled using bathymetric survey data. Five surface modelling approaches-Inverse Distance Weighting (IDW), Radial Basis Functions (RBF), Ordinary Kriging (OK), Universal Kriging (UK), and Empirical Bayesian Kriging (EBK)-were calibrated under a unified grid, extent, and neighbourhood design and assessed using leave-one-out cross-validation (LOOCV). Uncertainty was propagated via residual-bootstrap Monte Carlo simulation (10,000 realizations per method), and differences among methods were tested using ANOVA and Tukey's HSD ($p < 0.001$). EBK provided the most robust performance (RMSE = 0.569 m; $R^2 = 0.9806$), while OK minimized MAE (0.32 m); both showed near-zero bias. Comparison of the reconstructed reservoir-bed surfaces from 1987 and 2023 revealed substantial sediment accumulation and morphological changes within the reservoir basin. Updated elevation-volume relationships derived from the reliability-ranked EBK model indicate a total capacity loss of approximately 7.7 Mm³ (30.8%) since 1987 and near-complete infilling of dead storage (~97.5%). DEM-of-Difference (DoD) analysis revealed spatially heterogeneous sedimentation, with deposition reaching +8.26 m and localized erosion of up to -1.20 m. The proposed workflow provides practical quality control for bathymetric modelling and supports reliable assessment of reservoir sedimentation and capacity loss. The results can assist operational reservoir management and provide a scientific basis for planning sediment-removal and dredging activities.

Keywords: bathymetry, reservoir sedimentation, spatial interpolation, uncertainty propagation, capacity loss, DEM differencing

1. Introduction

Water reservoirs represent critical infrastructure for food security, drinking-water supply, hydropower production, and flood control. Their importance is particularly pronounced in arid and semi-arid regions, where stored water plays a fundamental role in buffering seasonal precipitation variability and limited natural inflows [1] and [2]. However, the long-term functionality and reliability of reservoirs are increasingly challenged by sedimentation processes, which progressively reduce storage capacity, impair hydraulic performance, and degrade water quality [3] and [4].

ISSN: 1686-6576 (Printed) | ISSN 2673-0014 (Online) | © Geoinformatics International

Sedimentation originates from catchment-scale soil erosion and the downstream transport of sediment particles such as sand, silt, and clay [5] and [6]. Although this process occurs naturally in fluvial systems, it is frequently accelerated by human activities including deforestation, construction, and unsustainable agricultural practices. These factors increase sediment yield within the basin and intensify reservoir infilling, potentially leading to ecological disturbance and operational challenges [7] and [8]. In many reservoirs worldwide, annual capacity losses reach approximately 1–2% of total storage, raising concerns about the long-term sustainability of existing water-storage infrastructure [4]. Consequently, accurate quantification of reservoir sedimentation has become an important prerequisite for sustainable reservoir operation and long-term water resources management. Furthermore, climate change is expected to intensify these dynamics through increasing precipitation variability, more frequent hydrological extremes, and ongoing land-cover changes, reinforcing the need for reliable monitoring and sedimentation assessment methods [9] and [10].

Accurate bathymetric mapping provides the fundamental basis for analysing reservoir sedimentation. Bathymetric surveys measure water depth along predefined transects and generate point datasets representing the submerged topography of the reservoir basin [11] and [12]. To estimate storage capacity and quantify morphological changes, these irregularly distributed measurements must be transformed into continuous bathymetric surfaces. Such surfaces enable the derivation of stage–area and stage–storage relationships, which are essential for reservoir operation, hydraulic modelling, and sedimentation assessment [13].

However, bathymetric measurements are rarely evenly distributed across the reservoir surface. Survey points are typically collected along navigation transects, leaving large unsampled areas between tracks. Consequently, spatial interpolation techniques are required to reconstruct the continuous bathymetric surface from discrete measurements. The choice of interpolation method plays a critical role in determining the realism and predictive accuracy of the resulting surface, and different interpolation approaches may lead to significantly different storage estimates [14] and [15].

In practice, two main groups of interpolation methods are widely used. Deterministic techniques, such as IDW and RBF, estimate unknown values based on weighted averages of nearby observations and are often favoured for their simplicity and computational efficiency [16] and [17].

However, these methods may be sensitive to clustering effects and can produce overly smooth surfaces. In contrast, geostatistical methods - including OK, UK and EBK - incorporate spatial autocorrelation structures through semivariogram modelling and provide statistical measures of prediction uncertainty [18] and [19]. Recent studies have also explored hybrid interpolation approaches and machine-learning-based methods, including Regression Kriging, Random Forest, and ensemble techniques, which have shown promising performance in geomorphological applications. However, these approaches generally require additional environmental covariates, extensive model calibration, and more complex computational workflows. Therefore, deterministic and classical geostatistical interpolation methods remain the most widely adopted techniques for routine bathymetric surveys and operational reservoir monitoring, particularly where only bathymetric observations are available.

Despite the widespread use of interpolation techniques in bathymetric studies, several important methodological gaps remain. Previous studies have primarily focused on comparing interpolation accuracy using individual validation metrics, while relatively little attention has been paid to uncertainty propagation and its influence on reservoir storage estimation. Moreover, only a limited number of studies have integrated cross-validation, uncertainty analysis, and statistical hypothesis testing into a unified framework for selecting the most appropriate interpolation method. These limitations reduce the reliability of bathymetric models used for estimating reservoir capacity and long-term sedimentation. To address these challenges, the present study develops an integrated evaluation framework that combines LOOCV, residual-bootstrap Monte Carlo simulation, ANOVA, and Tukey's HSD test to assess both interpolation accuracy and uncertainty.

This study focuses on Kamashi Reservoir in southern Uzbekistan using two datasets separated by 36 years. The historical reservoir-bed surface representing 1987 conditions was reconstructed from archived engineering topographic maps using a documented georeferencing and digitization workflow, whereas the contemporary dataset was obtained from a high-density hydrographic survey conducted in 2023. This methodological difference between historical reconstruction and direct bathymetric observation is acknowledged when interpreting long-term morphological changes. The objectives of the research are: (1) to construct a high-resolution bathymetric model for the 2023 survey using five spatial interpolation methods (IDW, RBF, OK, UK, and EBK) and identify the most reliable

approach using a unified validation framework; (2) to reassess the current storage condition of the reservoir and update stage - area and stage - volume relationships; (3) to reconstruct the historical 1987 bathymetric surface from archived design maps using a documented georeferencing and digitization workflow; and (4) to compare the 1987 and 2023 surfaces in order to identify spatial patterns of sediment deposition and erosion, quantify total storage loss, and describe long-term morphological changes within the reservoir basin.

Methodologically, interpolation performance is evaluated using LOOCV, while uncertainty propagation is assessed through Monte Carlo simulation with 10000 iterations. Statistical differences between interpolation methods are tested using Analysis of Variance (ANOVA), followed by Tukey's Honestly Significant Difference (Tukey HSD) test for pairwise comparisons. The best-performing interpolation surface is then used to estimate reservoir storage metrics and to generate a DEM-of-Difference map describing spatial patterns of morphological change.

The study contributes to reservoir sedimentation research by providing a reproducible and parameter-transparent workflow for bathymetric surface reconstruction in reservoirs with irregular morphologies. In addition, the paper presents updated storage estimates and a spatially explicit 36-year sedimentation assessment for Kamashi Reservoir, which may support reservoir monitoring and management in similar arid and semi-arid environments.

2. Methods and materials

2.1 Study Area and Dataset

Kamashi Reservoir is located in the Kamashi district of the Kashkadarya region in southern Uzbekistan, approximately 4 km from the district center (Figure 1). The reservoir was commissioned in 1987 after the construction of an earth-fill dam across the natural channel of the Shurchasoy River. Its main inflow is supplied through the 5.4 km long Kirabag Canal, which diverts water from the Yakkabog River originating on the southwestern slopes of the Gissar Range. The reservoir has a total storage capacity of about 25.0 Mm³, including 23.8 Mm³ of active storage and 1.2 Mm³ of dead storage allocated for sediment accumulation. At the normal water level (495.3 m.a.s.l.), the reservoir covers an area of approximately 3.82 km², while the earth-fill dam has a maximum height of 14.9 m and a crest length of 3,100 m.

Before digitization, the scanned maps were georeferenced in ArcGIS 10.8.3 using a first-order polynomial (Affine) transformation. Six well-distributed ground control points (GCPs) located on stable engineering structures, including three corners of the dam crest, a reference point on the concrete-lined water conveyance canal, a benchmark at the outlet structure, and a permanent feature upstream of the reservoir inflow, were used for georeferencing. The resulting georeferencing accuracy was RMSE = 0.94 m. Raster transformation was performed using the Nearest Neighbor resampling method to preserve the original raster values. After georeferencing, contour lines, spot elevations, and shoreline boundaries were manually digitized to reconstruct the historical reservoir-bed surface. The reconstructed elevations were validated against the original construction topographic survey control points, resulting in an estimated vertical accuracy of ±0.08 m.

Quality-control procedures were carried out before the bathymetric survey to ensure the reliability of depth measurements. The CHCNAV Apache-3 USV was equipped with a single-beam echo sounder operating at 200 kHz. Prior to data acquisition, the echo sounder was calibrated according to the manufacturer's standard procedures by verifying the transducer draft and comparing echo-sounder depth measurements with manual depth measurements obtained using a calibrated graduated sounding rod at four representative locations within the reservoir. The comparison confirmed a vertical accuracy of approximately ±0.05 m, and the calibration results were accepted before the survey commenced. Bathymetric positioning was provided by an integrated CHCNAV i90 GNSS RTK receiver. Because Kamashi Reservoir is an inland water body with stable water-level conditions during the survey, all measurements were referenced to the observed reservoir water level, and tidal corrections were not required. Depth measurements were collected at intervals of approximately 1–2 m along survey transects spaced at roughly 100 m. The lengths of transects varied between 150 m and 1,600 m depending on the local morphology of the reservoir basin (Figure 1).

The survey covered a total area of approximately 4.50 km². Of this area, 2.22 km² corresponded to open-water bathymetry, yielding 5,088 depth measurements with an average density of approximately 2,292 points km⁻². The remaining 2.28 km² included topographic measurements along the shoreline and dam abutments, producing 5,749 georeferenced points with an average density of approximately 2,521 points km⁻². In total, 10,837 survey points were collected, resulting in an overall measurement density of approximately 2,408 points km⁻². Coverage gaps remain only in extremely shallow or vegetated areas where navigation of the

ISSN: 1686-6576 (Printed) | ISSN 2673-0014 (Online) | © Geoinformatics International

survey platform was not possible. Two primary datasets were used in this study to evaluate morphological changes within the reservoir basin: (i) historical design maps from 1987 and (ii) bathymetric and topographic field surveys conducted in 2023.

The historical dataset consists of original engineering topographic maps prepared during the construction of the reservoir in 1987. The maps contain contour lines, spot elevations, shoreline boundaries, and hydraulic structures.

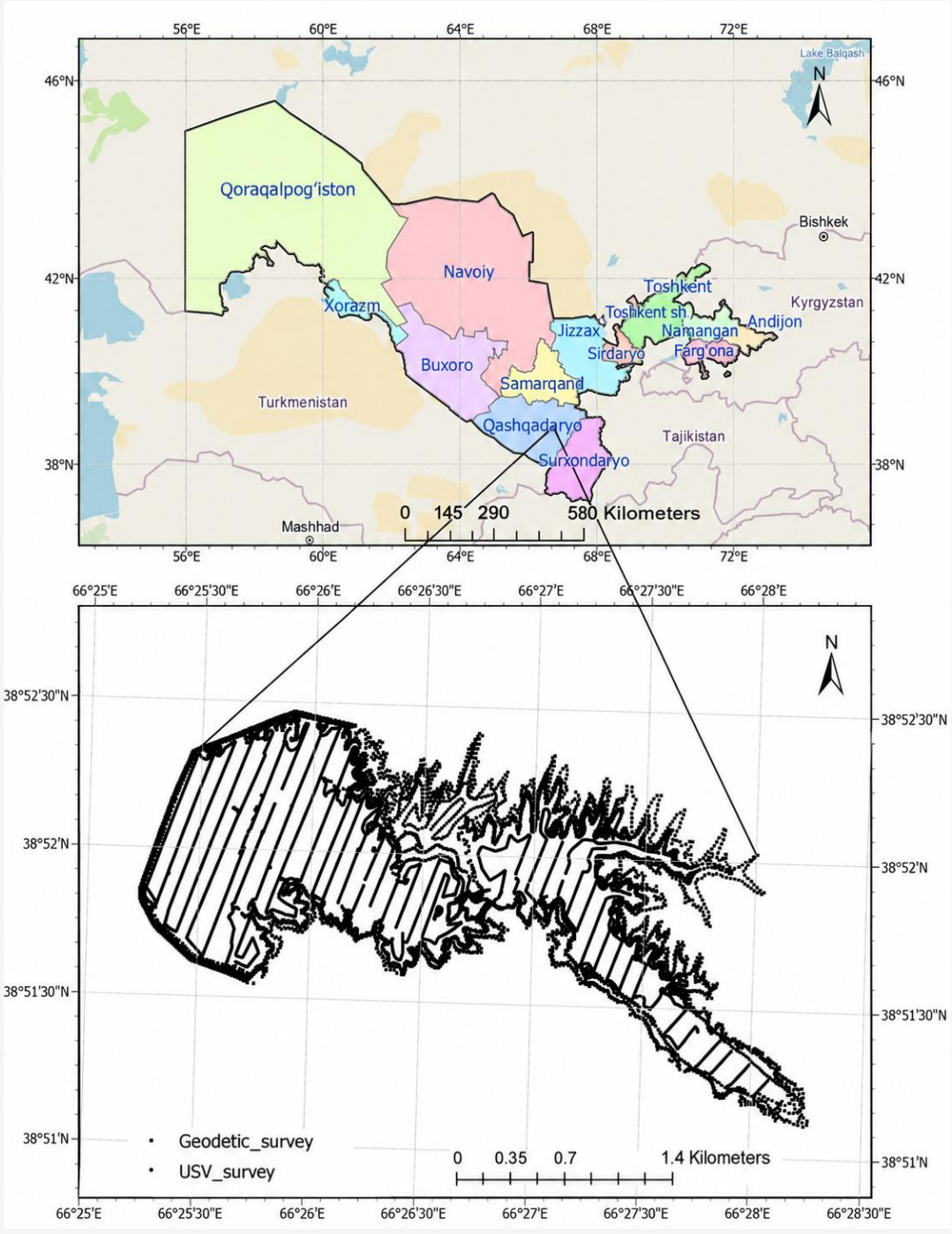


Figure 1: Location of Kamashi Reservoir within Uzbekistan (a) and spatial distribution of the 2023 bathymetric (USV) and topographic (GNSS) survey data collected during the field campaign (b)

2.2 Data Processing and Spatial Interpolation

2.2.1 Exploratory Spatial Data Analysis (ESDA)

Before spatial interpolation, the bathymetric dataset obtained during the 2023 survey was analysed using exploratory spatial data analysis (ESDA) to evaluate the statistical distribution of depth measurements, detect potential outliers, and assess spatial structure relevant for interpolation modelling [20]. The ESDA included descriptive statistical analysis, normality assessment, outlier detection, trend analysis, and evaluation of spatial autocorrelation. The summary statistics of the bathymetric dataset are presented in Table 1. The dataset consists of 10,837 bathymetric and topographic observations with elevations ranging from 482.992 m to 497.900 m. The calculated mean and median elevations are 491.729 m and 492.000 m, respectively, indicating only a slight difference between measures of central tendency. The distribution exhibits a skewness of −0.418 and an excess kurtosis of −0.854, suggesting a slightly negatively skewed distribution with relatively light tails. Formal normality assessment using the Shapiro–Wilk test rejected the null hypothesis of perfect normality ($p < 0.001$). However, considering the large sample size and the relatively small deviation from symmetry, no data transformation was applied prior to interpolation because geostatistical interpolation methods are generally robust to moderate departures from normality.

Potential outliers were evaluated using the 1.5 × interquartile range (IQR) criterion. No statistically significant outliers were identified; therefore, all observations were retained for subsequent interpolation and validation analyses.

Trend analysis revealed a pronounced longitudinal elevation gradient along the reservoir axis, reflecting the geomorphological configuration of the basin and long-term sediment deposition processes. The spatial distribution of the survey observations follows the bathymetric survey transects and provides adequate spatial coverage of both the inundated reservoir area and exposed shoreline zones.

Spatial dependence analysis demonstrated strong spatial autocorrelation among neighbouring observations, with similarity decreasing as separation distance increased. The elongated geometry of the reservoir also indicated the presence of directional anisotropy, which was subsequently incorporated into the geostatistical interpolation models through directional variogram analysis.

Overall, the ESDA results demonstrate a well-distributed dataset with no significant outliers, a clear spatial trend, and strong spatial dependence. These characteristics provided the basis for selecting appropriate interpolation methods and defining key modelling parameters, including neighbourhood configuration, anisotropy orientation, and variogram structure.

2.2.2 Selection and Parameterization of Spatial Interpolation Methods

Guided by the ESDA findings presented in Section 2.2.1, spatial interpolation was performed using the Geostatistical Analyst extension in ArcGIS 10.8.3. The ESDA diagnostics indicated that the bathymetric dataset follows an approximately normal distribution; therefore, no transformation of the depth values was required. Trend analysis revealed a clear longitudinal gradient along the main reservoir axis, suggesting that interpolation models capable of representing spatial drift should be considered.

Based on these characteristics, five interpolation techniques were selected representing two methodological groups: deterministic methods (IDW and RBF) and geostatistical methods (OK, UK, and EBK) [21] [22] and [23]. These methods are widely applied in bathymetric modelling and provide a representative comparison between deterministic approaches and geostatistical techniques that explicitly account for spatial dependence [24] and [25].

Table 1: Summary statistics of the 2023 bathymetric dataset used in the ESDA

Parameter	Value
Number of observations	10,837
Minimum elevation (m)	482.992
Maximum elevation (m)	497.900
Mean elevation (m)	491.729
Median elevation (m)	492.000
Standard deviation (m)	4.064
Skewness	−0.418
Excess kurtosis	−0.854
Shapiro–Wilk test	$p < 0.001$
Outlier detection (1.5 × IQR)	No outliers detected

To ensure comparability between interpolation models, identical spatial settings were applied across all methods. The interpolation grid size was defined according to the spatial density of survey measurements and set to approximately half of the median nearest-neighbour distance between observation points.

The interpolation extent was constrained using the reservoir water polygon as a spatial mask in order to prevent predictions outside the reservoir boundaries. A sector-based search neighbourhood oriented along the longitudinal axis of the reservoir was applied to account for directional spatial structure. In addition, shoreline boundaries were treated as barriers to avoid extrapolation beyond the reservoir limits.

For the IDW method, unsampled values were estimated as distance-weighted averages of neighbouring observations [26]. Several power values and neighbourhood configurations were evaluated during model calibration. Cross-validation identified a power value of 2.0 as the optimal configuration. Therefore, all final IDW interpolations were performed using a power parameter of 2.0 with 20 neighbouring observations distributed within four directional sectors.

The RBF method was applied to generate smooth deterministic surfaces under irregular sampling conditions [25]. Three kernel functions (multiquadric, Gaussian, and thin-plate spline) were evaluated during model calibration. Among these alternatives, the multiquadric kernel produced the lowest cross-validation error and was therefore selected for the final interpolation model.

For OK, spatial dependence was modelled using theoretical semivariogram functions [27]. Exponential, spherical, and Gaussian models were evaluated against the empirical semivariogram. The spherical variogram model provided the best cross-validation performance and was therefore adopted for the final interpolation. Directional anisotropy observed during ESDA was incorporated by orienting the variogram model parallel to the longitudinal axis of the reservoir.

Across all interpolation methods, the same spatial extent, grid resolution, neighbourhood configuration, and barrier constraints were maintained to ensure methodological consistency. The final parameter configuration for each interpolation method is summarized in Table 2, and all models were evaluated using the cross-validation procedure described in Section 2.3. UK was implemented to account for the large-scale spatial trend detected during ESDA [28]. A first-order polynomial trend was selected because the exploratory analysis indicated a predominantly linear longitudinal elevation gradient across the reservoir basin. Preliminary evaluation of higher-order polynomial trends did not produce meaningful improvements in cross-validation statistics while increasing model complexity; therefore, the first-order trend was retained. Finally, EBK was applied to address uncertainty in semivariogram parameter estimation and potential spatial non-stationarity [29]. EBK constructs multiple localized semivariogram models from subsets of the observations and combines them through Bayesian simulation, thereby reducing uncertainty associated with semivariogram estimation and improving prediction stability for heterogeneous bathymetric datasets.

2.3 Interpolation Accuracy Assessment

The predictive performance of the interpolation models was evaluated using an integrated validation framework that combines (i) point-based cross-validation, (ii) uncertainty and robustness assessment through Monte Carlo simulation, and (iii) formal hypothesis testing for differences among methods. This procedure provides a statistically defensible basis for selecting the most suitable interpolation surface for subsequent storage and morphological-change analyses.

Table 2: Final optimized parameter configuration of the spatial interpolation methods

Method	Final optimized parameters
IDW	Power = 2.0; 20 neighbouring observations; four-sector search neighbourhood; search ellipse aligned with the reservoir axis
RBF	Multiquadric kernel; 20 neighbouring observations
OK	Spherical variogram model; anisotropy incorporated along the reservoir axis
UK	First-order polynomial trend; spherical variogram model; same neighbourhood configuration as OK
EBK	Empirical transformation enabled; 100 simulations; subset size = 200; 20 neighbouring observations

2.3.1 Leave-One-Out Cross-Validation (LOOCV)

$nn-1i$ Interpolation accuracy was first assessed using LOOCV. For a dataset containing depth observations, each observation was sequentially removed and predicted using a model fitted to the remaining points. The predicted value was then compared with the measured value to form a validation residual [30] and [31]. For the -th observation:

$$e_i = M_i - \hat{M}_{-i}$$

Where M_i is the measured depth and $\hat{M}_{-i}$ is the LOOCV prediction at the same location produced by the model trained without point i. This process was repeated for all observations, yielding a complete residual set $\{e_i\}_{i=1}^{n}$ for each interpolation method.

Although LOOCV is widely used for spatial interpolation validation, it may provide slightly optimistic accuracy estimates when neighbouring observations exhibit strong spatial autocorrelation. Because adjacent bathymetric measurements are not completely independent, the reported validation statistics were interpreted as measures of relative model performance rather than absolute prediction accuracy. Nevertheless, LOOCV provides a consistent basis for comparing interpolation methods because the same validation procedure was applied to all models.

Cross-validation residuals were summarized using multiple accuracy indicators, selected because they capture complementary aspects of performance. The Root Mean Square Error (RMSE) is determined from Equation 1: it measures overall error magnitude and is sensitive to large deviations:

$$RMSE = \sqrt{\frac{1}{n}\sum_{i=1}^{n} e_i^2}$$

Equation 1

The Mean Absolute Error (MAE) is determined from Equation 2: it provides a robust measure of typical error magnitude:

$$MAE = \frac{1}{n}\sum_{i=1}^{n} | e_i |$$

Equation 2

R^2 the coefficient of determination is determined from Equation 3: it evaluates the agreement between measured and predicted values and reflects the proportion of variance explained by the model:

$$R^2 = 1 - \frac{\sum_{i=1}^{n}(M_i - \hat{M}_i)^2}{\sum_{i=1}^{n}(M_i - \bar{M})^2}$$

Equation 3

In addition, the dispersion of prediction errors was characterized using the standard deviation of the prediction residuals (SDpred), determined from Equation 4, which serves as a stability indicator (lower values imply more consistent predictions across the validation set):

$$SD_{pred} = \sqrt{\frac{1}{n-1}\sum_{i=1}^{n}(e_i - \bar{e})^2}$$

Equation 4

Where $\bar{e}$ is the mean of the residuals.

For geostatistical methods (OK, UK, EBK), calibration diagnostics were also inspected to ensure that not only the mean errors were small, but that the model uncertainty was realistic. In particular, standardized residuals were computed from Equation 5 as:

$$r_i = \frac{e_i}{\sigma_i}$$

Equation 5

Where σ_i is the kriging prediction standard error at location i. Well-calibrated kriging models typically show mean error close to zero and standardized residual dispersion close to unity (e.g., $ME \approx 0$, $MS \approx 0$, $RMSSE \approx 1$), and an approximate 95% coverage of standardized residuals within $[-1.96, 1.96]$ under near-normality. These checks were used as supporting evidence when selecting the best-performing surface among kriging-based models.

All validation statistics, including RMSE, MAE, R^2, and SD_{pred}, were calculated independently in Microsoft Excel using the cross-validation residuals exported from ArcGIS Geostatistical Analyst.

2.3.2 Residual-Bootstrap Monte Carlo Analysis for Robustness Assessment

To assess the robustness of the interpolation methods and quantify the uncertainty associated with interpolation residuals estimated from LOOCV, a residual-bootstrap Monte Carlo procedure was performed [32] and [33]. This approach propagates the variability of LOOCV residuals through repeated resampling and provides uncertainty intervals for the interpolation performance metrics. It should be noted that this procedure quantifies only the uncertainty associated with interpolation residuals and does not explicitly account for measurement errors, semivariogram uncertainty, shoreline delineation, or DEM harmonization errors. $\hat{M}(x_i)x_i\{e_i\}b = 1, \ldots, BB = 10000$ Let be the fitted value at observation location and let be the LOOCV residual

set for a given method. For iteration (with), residuals were resampled with replacement, following Equation 6:

$$e_i^{*(b)} \sim \{e_1, e_2, \dots, e_n\}$$

Equation 6

A pseudo-dataset was then generated from Equation 7 as:

$$M_i^{*(b)} = \widehat{M}(x_i) + e_i^{*(b)}$$

Equation 7

and a new bathymetric surface $\hat{Z}^{(b)}(x)$ was reconstructed using the same method settings (grid, mask, neighbourhood, and barriers).

During all Monte Carlo iterations, the interpolation parameters remained fixed at their optimized values determined through the cross-validation procedure (Section 2.2.2). Only the LOOCV residuals were resampled from their empirical distribution using simple random sampling with replacement, whereas all interpolation settings (including the power parameter, kernel function, variogram model, neighbourhood configuration, and search geometry) remained unchanged. This approach isolates the uncertainty associated with interpolation residuals while preserving the calibrated interpolation models. For each iteration, error metrics (e.g., RMSE and MAE) were recalculated using Equation 8, producing an empirical distribution of performance values for each method [34]:

$$\{RMSE^{(b)}\}_{b=1}^{B}, \{MAE^{(b)}\}_{b=1}^{B}$$

Equation 8

From these distributions, robustness was summarized using the mean and dispersion of the metric values and by reporting percentile-based 95% uncertainty intervals, following Equation 9:

$$CI_{95\%} = [Q_{0.025}, Q_{0.975}]$$

Equation 9

Methods exhibiting lower mean prediction errors together with narrower 95% residual-bootstrap confidence intervals were considered more robust with respect to interpolation residual variability. These uncertainty intervals should be interpreted only within the scope of residual-bootstrap analysis rather than as complete estimates of all sources of uncertainty affecting bathymetric reconstruction.

2.3.3 Statistical Comparison of Interpolation Methods (One-Way ANOVA and Tukey HSD)

$RMSE^{(b)}$ To determine whether differences in interpolation performance among the five interpolation methods were statistically significant, ANOVA was performed at a significance level of α = 0.05. The analysis was conducted using the iteration-wise error metrics obtained from the residual-bootstrap Monte Carlo simulations (e.g.,), providing a distributional basis for comparing interpolation methods rather than relying on a single validation statistic [33] and [35]. $y_{jb} j \in \{1, \dots, k\} b \in \{1, \dots, B\} k = 5$ Let denote the error metric (e.g., RMSE) for method at simulation iteration, where methods were compared (IDW, RBF, OK, UK, EBK). ANOVA tests the null hypothesis defined in Equation 10:

$$H_0: \mu_1 = \mu_2 = \cdots = \mu_k$$

Equation 10

against the alternative hypothesis that at least one group mean differed.

The ANOVA F-statistic was calculated from Equation 11 as

$$F = \frac{MS_{between}}{MS_{within}}$$

Equation 11

where $MS_{between}$ and MS_{within} denote the between-group and within-group mean squares, respectively. A statistically significant result ($p < 0.05$) indicated that not all interpolation methods produced equivalent prediction errors.

When ANOVA indicated significant overall differences, Tukey's Honestly Significant Difference (HSD) test was applied following Equation 12 for pairwise comparisons while controlling the family-wise error rate:

$$| \bar{y}_a - \bar{y}_b | \geq HSD$$

Equation 12

With Equation 13:

$$HSD = q_{\alpha;k;df} \sqrt{\frac{MS_{within}}{B}}$$

Equation 13

Where $q_{\alpha;k;df}$ is the Studentized range statistic, k is the number of methods, and df is the within-group degrees of freedom. This procedure identifies which specific method pairs differ significantly and supports an evidence-based ranking of interpolation techniques.

In addition to statistical significance, the effect size (η^2) was calculated from Equation 14 to quantify the proportion of the total variance explained by the interpolation method:

$$\eta^2 = \frac{SS_{between}}{SS_{total}}$$

Equation 14

Where $SS_{between}$ is the between-group sum of squares and SS_{total} is the total sum of squares.

2.3.4 Decision Rule for Selecting the Final Bathymetric Surface

The final interpolated bathymetric surface used for reservoir storage estimation and DEM-of-Difference (DoD) analysis was selected using a hierarchical multi-criteria decision framework. The primary selection criterion was the minimum Root Mean Square Error (RMSE) obtained from the LOOCV analysis, as RMSE provides a comprehensive measure of overall interpolation accuracy and is particularly sensitive to large prediction errors.

When two or more interpolation methods exhibited comparable RMSE values, additional evaluation criteria were considered to determine the final ranking. These included (i) lower Mean Absolute Error (MAE), (ii) higher coefficient of determination (R^2), (iii) lower residual dispersion (SD_{pred}), (iv) narrower 95% residual-bootstrap confidence intervals obtained from the Monte Carlo analysis, and (v) statistically significant differences identified by one-way ANOVA followed by Tukey's Honestly Significant Difference (HSD) test. For the geostatistical interpolation methods (OK, UK, and EBK), additional calibration diagnostics, including near-zero prediction bias and stable standardized residual behaviour, were also considered to ensure reliable model performance.

No independent validation dataset was available for external verification of the interpolation methods. Therefore, the final interpolation model was selected exclusively on the basis of the internal validation framework adopted in this study, which combined LOOCV, residual-bootstrap Monte Carlo analysis, and statistical comparison. This approach provides a consistent and reproducible basis for comparing interpolation methods under identical validation conditions.

Overall, the proposed decision framework provides a transparent, reproducible, and statistically supported procedure for selecting the interpolation method that most reliably represents the bathymetric morphology of the Kamashi Reservoir and is therefore suitable for subsequent storage estimation and long-term morphological change analysis

2.4 Estimation of Reservoir Storage and Analysis of Morphological Changes

The original 1987 engineering topographic maps were scanned at a resolution of approximately 600 dpi, mosaicked where necessary, and georeferenced in ArcGIS 10.8.3 using six well-distributed ground control points (GCPs). A first-order polynomial (Affine) transformation was applied, resulting in a georeferencing RMSE of 0.94 m, consistent with the georeferencing accuracy reported in Section 2.1. Subsequently, 26 contour lines and elevation points were digitized to reconstruct the historical reservoir topography. The digitized data were used to construct a Triangulated Irregular Network (TIN) using the Create TIN tool. The TIN was converted into a raster Digital Elevation Model (DEM) using the TIN to Raster tool with the Natural Neighbor interpolation method and a 2 m × 2 m cell size. A smoothing operation was subsequently applied to reduce minor interpolation artefacts while preserving the overall terrain morphology.

For comparative analysis, the 1987 and 2023 DEMs were harmonized to identical spatial conditions, including the same coordinate reference system, raster resolution, and spatial extent. Quality control procedures included visual inspection of the reconstructed DEMs, removal of isolated interpolation artefacts generated during raster conversion, application of the LoD threshold, and masking of uncertain shoreline cells prior to the DEM-of-Difference analysis.

Morphological changes were evaluated using a DEM of Difference (DoD) approach, defined in Equation 15:

$$\Delta Z(x,y) = Z_{2023}(x,y) - Z_{1987}(x,y) \quad \text{Equation 15}$$

Where $Z_{2023}$and Z_{1987}represent the reservoir bed elevations for the corresponding years. Positive values indicate sediment deposition, whereas negative values represent erosion.

To minimize the influence of insignificant elevation differences caused by measurement and interpolation uncertainty, a level of detection (LoD) threshold was applied following the propagated-error approach [37]: $LoD = t \cdot \sqrt{(\sigma^2 2023 + \sigma^2 1987)}$, where $\sigma 2023 = 0.569$ m is the EBK LOOCV RMSE (Table 3), $\sigma 1987 = 0.08$ m is the validated vertical accuracy of the digitized 1987 surface (Section 2.1), and $t = 1.96$ corresponds to the 95% confidence level. This yielded LoD = 1.13 m. Elevation differences with absolute values smaller than this threshold were considered within the uncertainty of the reconstructed surfaces and were therefore classified as noise and excluded from further analysis. Only elevation changes exceeding the LoD threshold were interpreted as actual sediment deposition or erosion. Sediment and erosion volumes were then calculated from Equation 16 by integrating elevation changes across the reservoir area:

$$V_{sed} = \sum_{i=1}^{n} A_i \cdot \Delta Z_i \quad \text{Equation 16}$$

where $A_i$is the raster cell area and ΔZ_irepresents elevation change. Reservoir storage capacity was evaluated by constructing elevation–area–volume (E–A–V) relationships for both 1987 and 2023 DEMs. The comparison of the resulting elevation–volume curves allowed quantification of storage capacity loss due to sediment accumulation.

Finally, longitudinal profiles along the reservoir thalweg and selected cross-sections were extracted to visualize spatial patterns of sediment deposition and morphological change.

3. Result

3.1 Comparison of Spatial Interpolation Surfaces

Figure 2 presents the bathymetric surfaces of the Kamashi Reservoir generated using five spatial interpolation methods: IDW, RBF, OK, UK and EBK. All interpolation models were produced using the same input dataset, spatial extent, raster resolution, and processing workflow to ensure direct comparison of the resulting bathymetric surfaces.

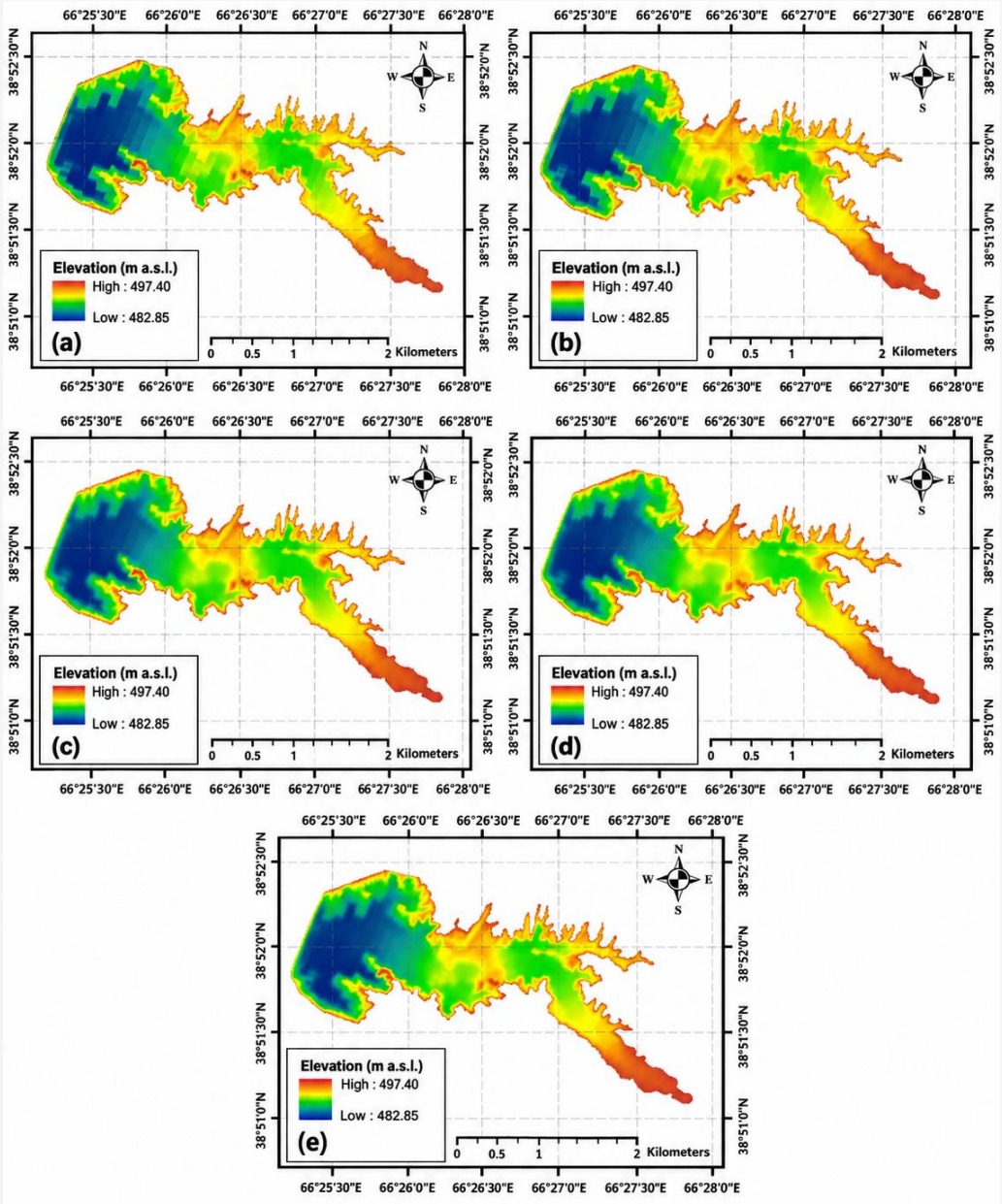


Figure 2: Comparison of bathymetric surfaces generated using five spatial interpolation methods: (a) IDW, (b) RBF, (c) OK, (d) UK, and (e) EBK. All maps were produced using identical raster resolution, spatial extent, and colour scale to facilitate direct visual comparison

ISSN: 1686-6576 (Printed) | ISSN 2673-0014 (Online) | © Geoinformatics International

Despite being generated from the same bathymetric observations, the interpolation methods produced noticeable differences in the representation of the reservoir bottom morphology. The IDW surface preserves the overall geometry of the reservoir while exhibiting localized angular transitions between neighbouring interpolated areas, particularly in regions characterized by abrupt depth variations. The RBF surface produces a more continuous representation of the bathymetric surface owing to its smoothing properties, resulting in gradual transitions between adjacent elevation zones.

The OK model reproduces the major bathymetric features while incorporating the spatial autocorrelation structure derived from the measured observations. Local bathymetric depressions and longitudinal depth variations remain identifiable throughout the reservoir. The UK model additionally incorporates the large-scale spatial trend detected during the exploratory spatial data analysis (Section 2.2.1), resulting in a representation that reflects both local spatial dependence and the longitudinal bathymetric gradient along the reservoir axis.

The EBK interpolation also preserves the principal morphological characteristics of the reservoir while representing local spatial variability throughout the basin. Differences among the five interpolation methods are most evident in areas characterized by complex shoreline geometry, steep bathymetric gradients, and rapidly changing depths, whereas the general reservoir morphology is consistently reproduced by all methods.

The visual comparison presented in Figure 2 illustrates the influence of different interpolation algorithms on the reconstructed bathymetric surface. However, visual inspection alone is insufficient to determine the most appropriate interpolation method. Therefore, quantitative evaluation using cross-validation statistics, residual-bootstrap Monte Carlo analysis, and statistical hypothesis testing is presented in the following sections.

3.2 Leave-One-Out Cross-Validation (LOOCV)

The predictive accuracy of each interpolation model was evaluated using LOOCV. In this procedure, each observation is sequentially removed from the dataset and predicted using the remaining data, and the predicted value is then compared with the measured elevation.

EBK achieved the lowest RMSE (0.569 m) and the highest coefficient of determination (R^2 = 0.9806), indicating the best overall predictive performance. OK produced a very similar RMSE (0.587 m) but achieved the lowest MAE (0.32 m), suggesting slightly better performance in terms of absolute error magnitude. Deterministic approaches produced substantially higher errors, with RMSE values of 0.957 m for RBF and 0.993 m for IDW. UK performed worst among the tested models, with an RMSE of 1.073 m and the lowest R^2 value.

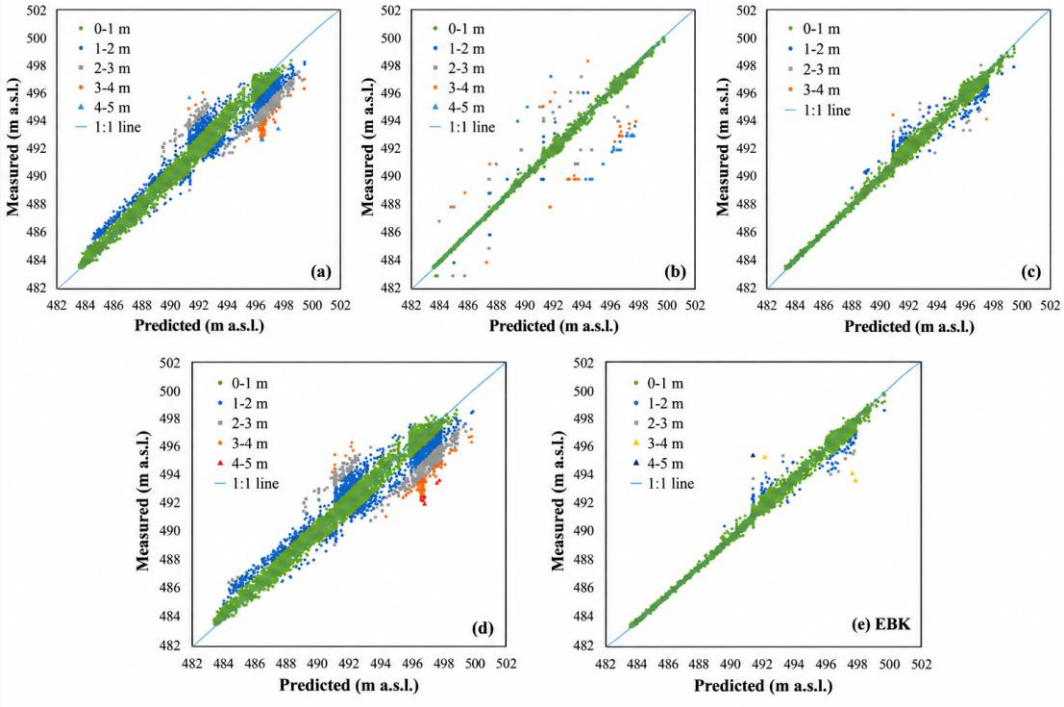


Figure 3: Measured vs. predicted elevation scatter plots (LOOCV): (a) RBF, (b) IDW, (c) OK, (d) UK, and (e) EBK

Table 3 summarizes the resulting accuracy statistics, including bias, MAE, RMSE, and R^2. The results clearly indicate that geostatistical interpolation methods outperform deterministic approaches. Scatter plots of measured versus predicted elevations (Figure 3) further illustrate these differences. Predictions generated by EBK and OK align closely with the 1:1 reference line, whereas deterministic methods exhibit larger deviations, particularly at the upper and lower ends of the elevation range.

3.3 Uncertainty Analysis Using Monte Carlo Simulation

To evaluate model robustness and quantify prediction uncertainty, residual bootstrap Monte Carlo simulations were performed for each interpolation method. For each model, 10,000 realizations were generated by resampling LOOCV residuals and slightly perturbing interpolation parameters around the optimal settings. The resulting RMSE distributions are summarized in Table 4. EBK exhibits the lowest mean RMSE (0.569 m) and the narrowest uncertainty range (P5–P95), indicating the most stable predictive performance. OK shows similar accuracy but slightly larger dispersion. Deterministic methods (RBF and IDW) display broader RMSE distributions, while UK shows both the highest mean error and the widest uncertainty range. These findings are illustrated in the RMSE distribution histograms shown in Figure 4.

3.4 Statistical Comparison of Interpolation Methods

To determine whether the differences in prediction accuracy between interpolation methods are statistically significant, the RMSE samples obtained from the Monte Carlo simulations were analysed using ANOVA. This approach was chosen because the RMSE distributions showed unequal variances across methods. The ANOVA results indicate a highly significant difference among interpolation methods ($F(4, \approx 24{,}355) = 1.19 \times 10^5$, $p < 0.001$), confirming that interpolation choice significantly affects predictive accuracy (Table 5).

Table 3: Summary of LOOCV statistics for each interpolation method

Method	Bias (m)	MAE (m)	MAE (%)	RMSE (m)	RMSE (%)	R^2
IDW	−0.104	0.58	0.12	0.993	0.2	0.95
RBF	−0.002	0.48	0.09	0.958	0.2	0.96
OK	−0.023	0.32	0.06	0.587	0.12	0.98
UK	0.00	0.55	0.11	1.073	0.22	0.89
EBK	−0.00	0.37	0.07	0.569	0.116	0.98

Table 4: Summary of MCS results

Method	Mean RMSE (m)	SD (m)	P5 (m)	P95 (m)
EBK	0.5689	0.0452	0.4945	0.6429
OK	0.5877	0.0501	0.5065	0.6705
RBF	0.9570	0.0793	0.8286	1.0887
IDW	0.9923	0.0904	0.8444	1.1390
UK	1.1007	0.1100	0.9181	1.2825

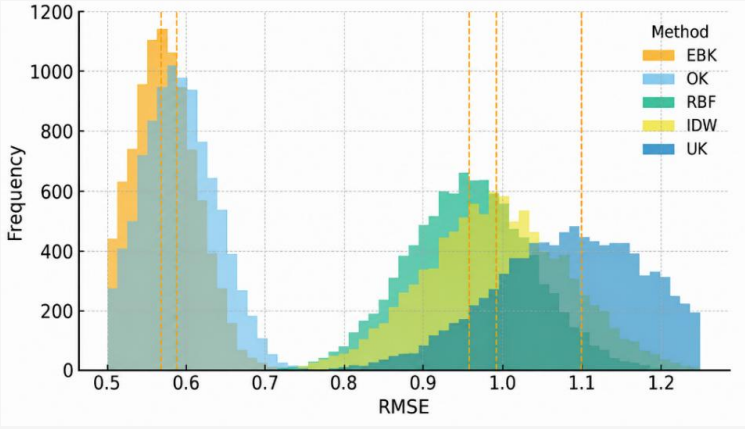


Figure 4: Monte Carlo Simulation Histogram

To identify which methods, differ significantly from one another, pairwise comparisons were conducted using Tukey's HSD test. The results (Table 6 and Figure 5) show that all pairwise differences are statistically significant. However, the difference between EBK and OK is relatively small (approximately 0.019 m), whereas differences between kriging-based and deterministic methods are considerably larger. For example, EBK shows a substantial improvement over IDW (+0.423 m RMSE difference) and UK (+0.532 m). OK demonstrates a similar advantage over deterministic approaches. Among the deterministic methods, RBF performs slightly better than IDW, while UK exhibits the lowest overall performance. These results establish the following performance ranking:
EBK > OK > RBF > IDW > UK

Table 5: One-way ANOVA for RMSE across interpolation methods (IDW, RBF, OK, UK, EBK)

Source	df	F	p-value
Between methods	4	1.19×10^{5}	<0.001
Within (ANOVA)	≈24,355	-	-

Table 6: Tukey HSD Test Results Based on MCS

Comparison (A vs B)	Mean diff (m)	95% CI (m)	Adj. p	Significant?
EBK vs OK	**0.019**	[0.017, 0.020]	<0.001	Yes
EBK vs RBF	0.388	[0.386, 0.390]	<0.001	Yes
EBK vs IDW	0.423	[0.421, 0.425]	<0.001	Yes
EBK vs UK	0.532	[0.529, 0.534]	<0.001	Yes
OK vs RBF	0.369	[0.367, 0.371]	<0.001	Yes
OK vs IDW	0.405	[0.403, 0.407]	<0.001	Yes
OK vs UK	0.513	[0.511, 0.515]	<0.001	Yes
RBF vs IDW	0.035	[0.033, 0.038]	<0.001	Yes
RBF vs UK	0.144	[0.141, 0.146]	<0.001	Yes
IDW vs UK	0.108	[0.106, 0.111]	<0.001	Yes

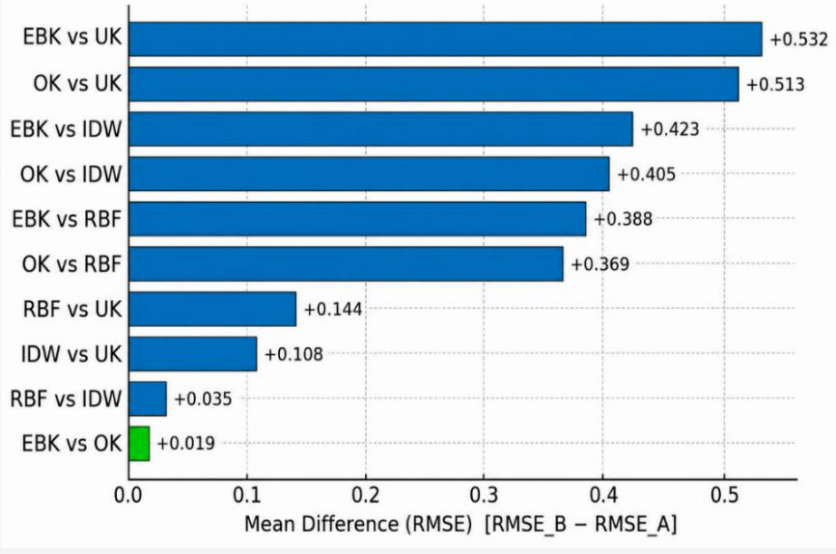


Figure 5: Tukey HSD test: Mean Differences (RMSE) between interpolation method Pairs

3.5 Estimation of Reservoir Storage and Analysis of Volume Changes Over Time

Based on the accuracy assessment, EBK was selected as the most reliable interpolation method for further bathymetric modelling. Using the EBK-derived surface, a three-dimensional bathymetric model of the Kamashi Reservoir was constructed to represent the current bed conditions in 2023 (Figure 6). The model reveals a pronounced sediment accumulation zone in the central part of the reservoir, forming a prominent sediment mound within the elevation range of approximately 491–492 m. This depositional feature has effectively divided the reservoir into two functional sections, altering internal flow paths and potentially affecting hydraulic conditions. Elevation–volume (H–V) relationships derived from the 2023 bathymetric model were compared with the original design curve from 1987 (Figure 7). The comparison indicates a substantial decline in reservoir capacity. Over 36 years of operation, the total storage volume decreased by approximately 7.7 million m³, corresponding to a 30.8% reduction in storage capacity.

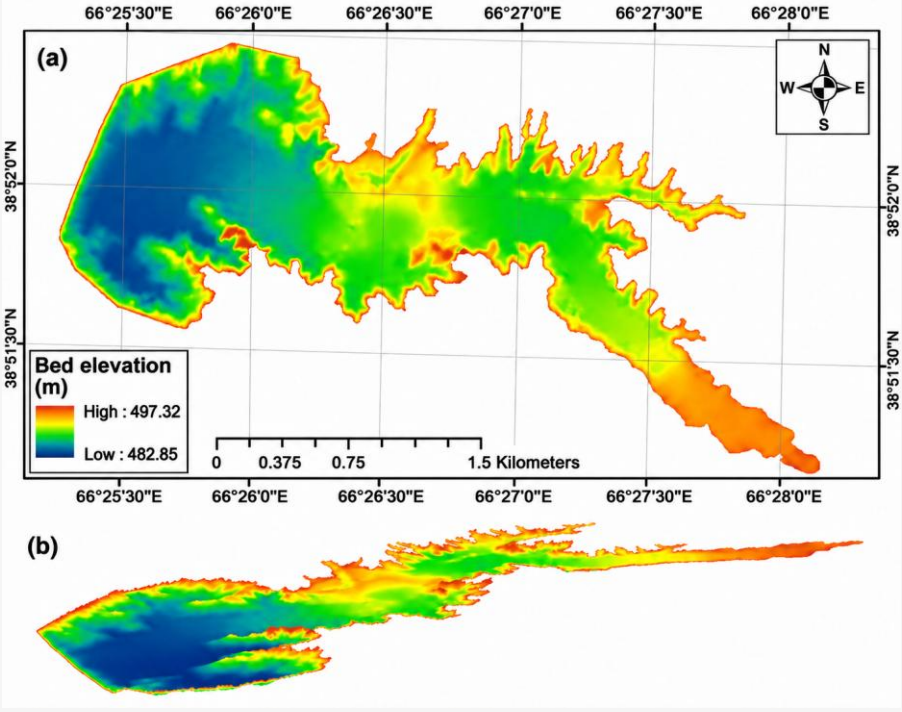


Figure 6: Reservoir Bathymetric Map and 3D Spatial Model for 2023: (a) 2D bathymetric surface map; (b) 3D perspective view of the reservoir bed

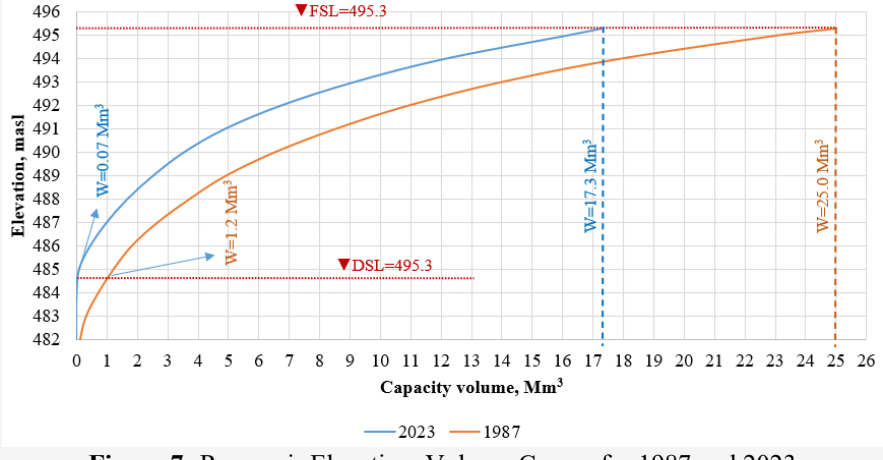


Figure 7: Reservoir Elevation–Volume Curves for 1987 and 2023

In addition, the reservoir surface area increased by approximately 0.68 km², reflecting sediment spreading and delta formation in shallow areas. The dead storage zone, originally designed to accommodate 1.2 million m³ of sediment, is now almost completely filled, with approximately 97.5% of its capacity lost due to sediment accumulation.

3.6 Reservoir Morphological Changes

Morphological changes in the Kamashi Reservoir were analysed by comparing digital elevation models representing the reservoir bed conditions in 1987 and 2023 (Figure 8). The DEM differencing results reveal extensive sediment deposition, particularly concentrated in the upstream inflow zone and the central basin.

The elevation difference map indicates sediment accumulation of up to +8.26 m, while localized erosion areas reach approximately –1.20 m. These patterns are further illustrated in the three-dimensional morphological model, which highlights asymmetric sediment distribution and the formation of a large sediment body in the central part of the reservoir.

Longitudinal bed profiles extracted along the reservoir axis (Figure 9) confirm a progressive increase in bed elevation between 1987 and 2023, particularly in the mid-basin section. This sediment accumulation has reduced the effective water depth and expanded the dead storage zone, thereby decreasing the hydraulic efficiency of the reservoir.

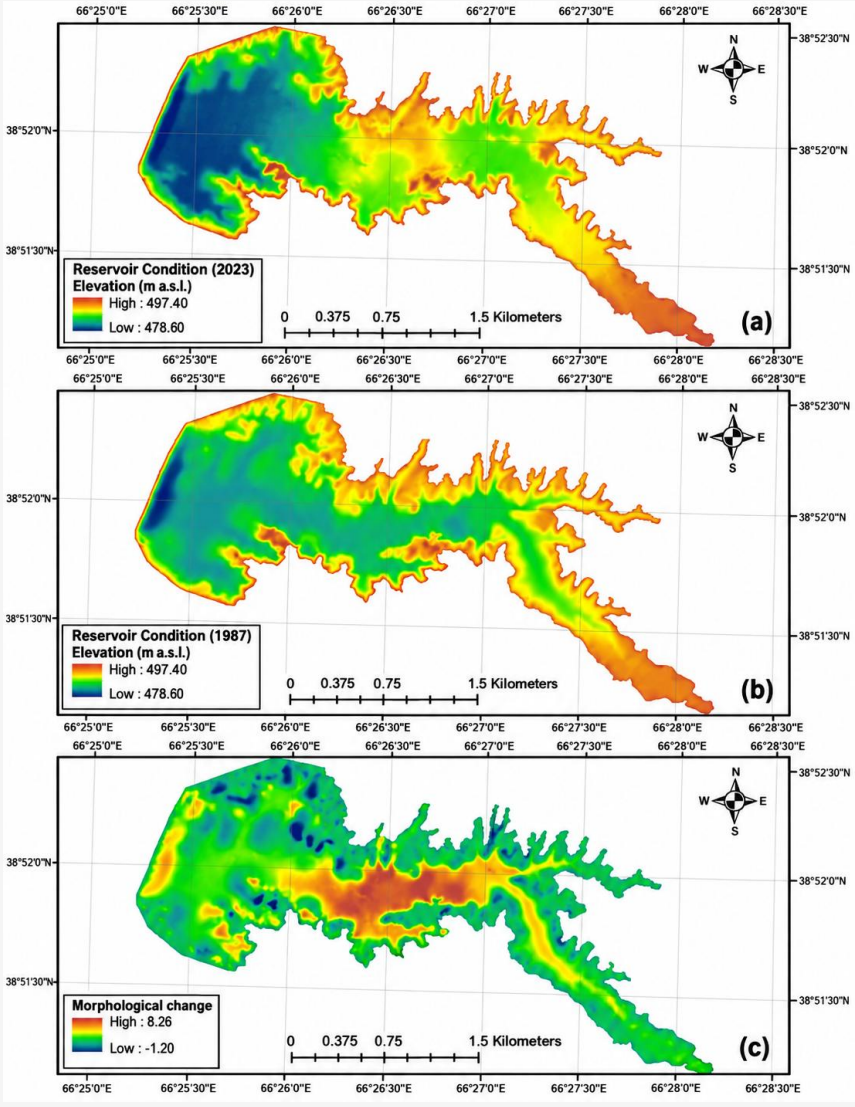


Figure 8: Comparison of reservoir bed conditions in 1987 and 2023 and the resulting morphological changes: (a) reservoir bed condition in 2023, (b) reservoir bed condition in 1987, and (c) spatial distribution of bed-elevation changes between 1987 and 2023

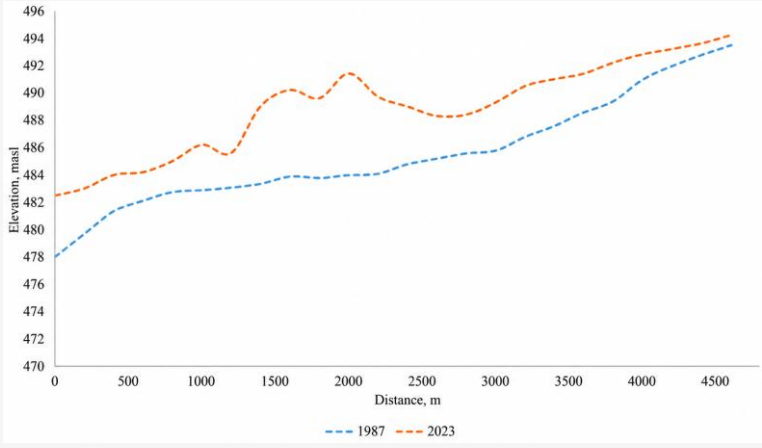


Figure 9: Longitudinal bed profiles of the reservoir for 1987 and 2023

The high concentration of fine sediments in the central basin is primarily associated with inflows from the Korabog Canal, which delivers sediment-laden water directly into this part of the reservoir. Continuous sediment input from this canal has therefore played a major role in the long-term morphological transformation of the reservoir.

4. Discussion

The results demonstrate the effectiveness of geostatistical interpolation methods for reconstructing bathymetric surfaces and analysing reservoir sedimentation processes. Among the five tested interpolation approaches (IDW, RBF, OK, UK, and EBK), the EBK method consistently achieved the highest predictive accuracy and robustness, as confirmed by LOOCV validation, Monte Carlo uncertainty analysis, and statistical comparison using ANOVA and Tukey's HSD tests. The superior performance of EBK reflects its ability to account for uncertainty in semivariogram estimation and to better represent spatial dependence within heterogeneous bathymetric datasets.

The spatial modelling results reveal a clear pattern of sediment accumulation in the Kamashi Reservoir. In particular, the formation of a large sediment mound in the central basin represents a significant morphological transformation of the reservoir bed. This depositional structure effectively divides the reservoir into two functional sub-basins and alters internal flow pathways. Such morphological restructuring may influence water circulation patterns, sediment transport pathways, and hydraulic efficiency of the reservoir.

The observed storage loss of approximately 7.7 million m³ (30.8%) over 36 years indicates substantial long-term sediment accumulation. Similar trends have been reported in other reservoirs where sediment inflow from tributaries and irrigation canals accelerates capacity loss. However, the spatially explicit bathymetric modelling conducted in this study provides additional insight into the internal distribution of sediment deposits and their morphological implications.

The findings both align with and extend previous studies. For example, sedimentation in the Akdarya Reservoir has similarly been analysed using turning bands simulation combined with kriging to estimate probabilistic storage intervals [36]. That approach provided valuable probabilistic estimates of storage capacity, but it offered limited visualization of spatial sediment distribution. In contrast, the present study integrates DEM differencing, three-dimensional bathymetric modelling, and longitudinal bed profiling, enabling a clearer representation of how sediment accumulation physically reshapes the reservoir morphology.

Interpolation techniques combined with LOOCV and Monte Carlo simulations have also been applied to evaluate bathymetric changes in the Tucuruí Reservoir, Brazil [11], a substantially larger and more frequently monitored reservoir with a different survey design and validation approach; that analysis primarily focused on operational monitoring using area–volume relationships. The current study extends this methodological framework by incorporating spatially explicit bathymetric surfaces and DEM differencing, which allow detailed identification of sediment deposition zones and morphological transformation patterns.

Sedimentation processes in the Abrajit Dam have similarly been assessed, with watershed management recommendations proposed [38]. That analysis relied mainly on volumetric estimates and did not include detailed spatial modelling of sediment distribution. In contrast, the spatial coincidence between the Korabog Canal inflow and the central sediment body observed in the present study suggests, but does not by itself confirm, a causal link between canal-derived sediment loads and this depositional feature; the

identification of this pattern highlights the importance of considering canal-derived sediment loads when designing sediment management strategies.

These findings are also consistent with sediment-driven capacity losses documented in other Uzbek reservoirs by our research group. The Tuplang Reservoir lost 28.05 Mm³ (5.65% of total volume) over more than three decades, concentrated in the dead-storage zone between 830 and 890 m a.s.l. [6], while the Akhangaran Reservoir lost 28.6 Mm³ (14.44%) over 50 years, including a 55.73% reduction in dead volume [13]. More recently, the Hisorak Reservoir was found to have lost 39.4 Mm³ (23.2%) of its storage capacity over 42 years, at an average sedimentation rate more than three times the original design estimate [39]. Compared with these cases, the Kamashi Reservoir's 30.8% capacity loss and near-complete (~97.5%) infilling of dead storage since 1987 indicate a comparatively severe sedimentation regime, likely reflecting differences in catchment sediment yield, inflow-canal design, and reservoir operation among these systems.

A key advantage of geostatistical interpolation—particularly EBK—is its ability to model spatial autocorrelation through variogram-based analysis. This capability improves the accuracy of surface reconstruction and allows reliable estimation of morphological changes within reservoir basins. The combination of EBK interpolation with Monte Carlo uncertainty analysis and statistical testing therefore provides a robust framework for bathymetric modelling and sedimentation assessment.

Although the present study provides a detailed spatial analysis of sedimentation processes, some limitations should be acknowledged. First, the 1987 and 2023 datasets differ substantially in their method of acquisition: the 1987 surface was reconstructed from digitized historical engineering maps with a validated vertical accuracy of ±0.08 m, whereas the 2023 surface is a direct high-density USV survey; this asymmetry means that the reported 36-year change reflects both genuine morphological change and residual differences in data-source precision, so the resulting capacity-loss estimate should be read as a best estimate rather than an exact figure. Second, the analysis relies on only two temporal datasets, which limits the ability to capture intermediate stages of sediment evolution; future studies could incorporate multi-temporal bathymetric surveys or remote sensing observations to better quantify sedimentation dynamics over time. Third, as noted in Section 2.3.2, the Monte Carlo uncertainty analysis quantifies only the uncertainty associated with interpolation residuals and does not explicitly propagate measurement errors, semivariogram uncertainty, or DEM harmonization errors into the final capacity-loss estimate; probabilistic approaches such as turning bands simulation or stochastic reservoir sedimentation models could further improve this assessment in future work.

Overall, the integration of geostatistical interpolation, uncertainty analysis, and DEM-based morphological assessment provides a powerful methodology for evaluating sediment accumulation and reservoir capacity loss. The results highlight the importance of continuous sediment monitoring, management of sediment-laden inflows, and implementation of targeted sediment mitigation strategies. Such approaches are essential for sustaining reservoir functionality and ensuring long-term water resource security in sediment-prone basins.

5. Conclusion

This study evaluated the predictive accuracy of five spatial interpolation methods (IDW, RBF, OK, UK, and EBK) for reconstructing reservoir bathymetry. Using a unified validation framework combining LOOCV, Monte Carlo simulation, ANOVA, and Tukey's HSD, EBK was identified as the most accurate and robust method, providing the lowest RMSE and the narrowest uncertainty range. OK showed comparable performance with the lowest MAE and near-zero bias, making it a reliable alternative. Deterministic methods produced smoother but less accurate surfaces, while UK performed weakest under strong local variability.

Although statistical tests confirmed significant differences between all interpolation methods, the RMSE difference between EBK and OK was small (~1.9 cm), indicating that both methods provide highly reliable bathymetric reconstructions.

Based on the EBK-derived surface, reservoir capacity analysis indicates a 7.7 Mm³ (30.8%) reduction in total storage since 1987, with approximately 97.5% of the dead storage filled by sediments; because the 1987 baseline was reconstructed from digitized historical maps rather than a direct survey, this percentage should be read as a best estimate rather than a precise figure. DEM differencing (applying a level-of-detection threshold of 1.13 m) further revealed dominant sediment accumulation, with deposition reaching +8.26 m in some areas - well above the detection threshold and therefore a reliable finding - while the localized erosion values of up to −1.20 m lie close to the detection threshold and should be interpreted with caution.

Overall, the results demonstrate that EBK is the most reliable method for bathymetric surface reconstruction, while OK provides a strong

alternative. Accurate interpolation is essential for reliable estimation of reservoir capacity and for understanding sediment-driven morphological changes.

Acknowledgments
LLC "Center for Safety Assessment and Monitoring of Hydrotechnical Facilities" generously provided bathymetric data. We thank all members of the hydrographic survey crew for their field support. We also acknowledge JSC "Uzbekgidrenergo" and its affiliated organization "Akhangaran GES" for supplying historical bathymetric and related datasets. In addition, we extend our special gratitude to the Joint Center for Geoinformatics at TIIAME NRU for technical guidance, computational resources, and constructive feedback.

Author Contributions
Khojiakbar Khasanov contributed to conceptualization, methodology, formal analysis, investigation, visualization, writing original draft preparation, and writing review and editing. Masharif Bakiev contributed to supervision, conceptualization, methodology, and writing review and editing. Shakhnoza Djabbarova contributed to data curation, software, and investigation. Ozoda Vafoeva contributed to field investigation, data collection, and validation. Kamola Rakhmatilloyeva contributed to software and data processing. Gulnoza Mulladjanova contributed to visualization and data processing. All authors have read and agreed to the published version of the manuscript.

References

[1] Rakhmatullaev, S., Huneau, F., Celle-Jeanton, H., Le Coustumer, P., Motelica-Heino, M. and Bakiev, M., (2013). Water Reservoirs, Irrigation and Sedimentation in Central Asia: a First-Cut Assessment for Uzbekistan. *Environmental Earth Sciences*. Vol. 68; 985-998. https://doi.org/10.1007/s12665-012-1802-0

[2] Zhao, G., Liu, S., Deng, H., Tang, Q., Zhang, C., Su, Y. and Chen, F., (2025). Identifying Drivers of Storage Dynamics of Lakes and Reservoirs in the Arid Central Asia. *Environmental Research Letters*. Vol. 20(1). https://doi.org/10.1088/1748-9326/ad975b

[3] Morris, G. L., (2020). Classification of Management Alternatives to Combat Reservoir Sedimentation. *Water*. Vol. 12(3). https://doi.org/10.3390/w12030861

[4] Perera, D., Williams, S. and Smakhtin, V., (2023). Present and Future Losses of Storage in Large Reservoirs Due to Sedimentation: a Country-Wise Global Assessment. *Sustainability*. Vol. 15(1); 219. https://doi.org/10.3390/su15010219

[5] Rodriguez, L., McCallum, A., Kent, D., Rathnayaka, C. and Fairweather, H., (2023). A Review of Sedimentation Rates in Freshwater Reservoirs: Recent Changes and Causative Factors. *Aquatic Sciences*. Vol. 85(2). https://doi.org/10.1007/s00027-023-00960-0

[6] Khasanov, K. and Bakiev, M., (2025). GIS-Based Geostatistical Techniques for Sedimentation Assessment Using USV Data: Case Study Tuplang Reservoir, Uzbekistan. *International Journal of Engineering and Geosciences*. Vol. 10(2); 231-243. https://doi.org/10.26833/ijeg.1567019

[7] Regasa, M. S. and Nones, M., (2023). SWAT Model-Based Quantification of the Impact of Land Use Land Cover Change on Sediment Yield in the Fincha Watershed, Ethiopia. *Frontiers in Environmental Science*. Vol. 11. https://doi.org/10.3389/fenvs.2023.1146346

[8] Bihonegn, B. G. and Awoke, A. G., (2023). Evaluating the Impact of Land Use and Land Cover Changes on Sediment Yield Dynamics in the Upper Awash Basin, Ethiopia the Case of Koka Reservoir. *Heliyon*. Vol. 9(12); e23049. https://doi.org/10.1016/j.heliyon.2023.e23049

[9] Zhang, T., Li, D., East, A. E., Kettner, A. J., Best, J., Ni, J. and Lu, X., (2023). Shifted Sediment-Transport Regimes by Climate Change and Amplified Hydrological Variability in Cryosphere-Fed Rivers. *Science Advances*. Vol. 9(45). https://doi.org/10.1126/sciadv.adi5019

[10] Khasanov, K., Babajanova, N., Chymyrov, A., Reyimov, D. and Salokhitdinova, S., (2024). Geostatistical Approach in Estimating the Capacity Volume of the Mudflow Reservoir. *E3S Web of Conferences*, Vol. 590, EDP Sciences. https://doi.org/10.1051/e3sconf/202459007003

[11] Curtarelli, M., Leão, J., Ogashawara, I., Lorenzzetti, J. and Stech, J., (2015). Assessment of Spatial Interpolation Methods to Map the Bathymetry of an Amazonian Hydroelectric Reservoir to Aid in Decision Making for Water Management. *ISPRS International Journal of Geo-Information*. Vol. 4(1); 220-235. https://doi.org/10.3390/ijgi4010220

[12]Mansouri, I., Bengora, D. and Houichi, L., (2024). Enhancing Reservoir Dam's Management in Algeria: a Comparative Study of Interpolation Methods for Topo-Bathymetric Surveys. *Modeling Earth Systems and Environment*. Vol. 10(1); 943-955. https://doi.org/10.1007/s40808-023-01816-0

[13]Khasanov, K., (2025). A Comprehensive Analysis of Reservoir Capacity Loss: a Case Study of the Akhangaran Reservoir, Uzbekistan. *Water Cycle*. Vol. 6; 105-117. https://doi.org/10.1016/j.watcyc.2024.11.003

[14]Arseni, M., Voiculescu, M., Georgescu, L. P., Iticescu, C. and Rosu, A., (2019). Testing Different Interpolation Methods Based on Single Beam Echosounder River Surveying. Case Study: Siret River. *ISPRS International Journal of Geo-Information*. Vol. 8(11); 507. https://doi.org/10.3390/ijgi8110507

[15]Amoroso, P. P., Aguilar, F. J., Parente, C. and Aguilar, M. A., (2023). Statistical Assessment of Some Interpolation Methods for Building Grid Format Digital Bathymetric Models. *Remote Sensing*. Vol. 15(8); 2072. https://doi.org/10.3390/rs15082072

[16]Li, J. and Heap, A. D., (2014). Spatial Interpolation Methods Applied in the Environmental Sciences: a Review. *Environmental Modelling & Software*. Vol. 53; 173-189. https://doi.org/10.1016/j.envsoft.2013.12.008

[17]Lu, G. and Wong, D., (2008). An Adaptive Inverse-Distance Weighting Spatial Interpolation Technique. *Computers & Geosciences*. Vol. 34; 1044-1055. https://doi.org/10.1016/j.cageo.2007.07.010

[18]Ogryzek, M., Krypiak-Gregorczyk, A. and Wielgosz, P., (2020). Optimal Geostatistical Methods for Interpolation of the Ionosphere: a Case Study on the St Patrick's Day Storm of 2015. *Sensors*. Vol. 20. https://doi.org/10.3390/s20102840

[19]Biernacik, P., Kazimierski, W. and Włodarczyk-Sielicka, M., (2023). Comparative Analysis of Selected Geostatistical Methods for Bottom Surface Modeling. *Sensors*. Vol. 23. https://doi.org/10.3390/s23083941

[20]Dall'erba, S. and Chen, Z., (2020). Exploratory Spatial Data Analysis. In: Kobayashi, A., editor. *International Encyclopedia of Human Geography (Second Edition)*, Second Edition, Oxford: Elsevier, p. 357-365. https://doi.org/10.1016/B978-0-08-102295-5.10541-4

[21]Kebede, H., Demissie, Z., Tadesse, H. and Eshetu, A., (2024). Spatial Interpolation Techniques Comparison and Evaluation: the Case of Ground-Based Gravity and Elevation Datasets of the Central Main Ethiopian Rift. *Heliyon*. Vol. 10. https://doi.org/10.1016/j.heliyon.2024.e32806

[22]Wu, C., Mossa, J., Mao, L. and Almulla, M., (2019). Comparison of Different Spatial Interpolation Methods for Historical Hydrographic Data of the Lowermost Mississippi River. *Annals of GIS*. Vol. 25(2); 133-151. https://doi.org/10.1080/19475683.2019.1588781

[23]Mahabub, M., Alam, M. M. and Nuruzzaman, M., (2025). Comparative Analysis of Interpolation Methods Commonly Used in Bathymetric Data Generation. *World Journal of Advanced Research and Reviews*. https://doi.org/10.30574/wjarr.2025.25.3.0835

[24]Pratomo, D., Safira, R. A. D. and Stefani, O., (2023). A Comparison of Different GIS-Based Interpolation Methods for Bathymetric Data: Case Study of Bawean Island, East Java. *Geodesy and Cartography*. https://doi.org/10.3846/gac.2023.18250

[25]Ndou, N., Nontongana, N., Thamaga, K. H. and Afuye, G. A., (2024). Uncertainty Evaluation and Compensation for Reservoir's Bathymetric Patterns Predicted with Radial Basis Function Approaches Based on Conventionally Acquired Water Depth Data. *Water*. Vol. 16(21); 3052. https://doi.org/10.3390/w16213052

[26]Ikechukwu, M., Ebinne, E., Idorenyin, U. and Raphael, N., (2017). Accuracy Assessment and Comparative Analysis of IDW, Spline and Kriging in Spatial Interpolation of Landform (Topography): an Experimental Study. *Journal of Geographic Information System*. Vol. 9; 354-371. https://doi.org/10.4236/jgis.2017.93022

[27]Maiti, P. and Mitra, D., (2022). Complexity Reduction of Ordinary Kriging Algorithm for 3D REM Design. *Physical Communication*. Vol. 55; 101912. https://doi.org/10.1016/j.phycom.2022.101912

[28]Alcaras, E., Amoroso, P. and Parente, C., (2022). The Influence of Interpolated Point Location and Density on 3D Bathymetric Models Generated by Kriging Methods: an Application on the Giglio Island Seabed (Italy). *Geosciences*. Vol. 12(2); 62. https://doi.org/10.3390/geosciences12020062

[29]Krivoruchko, K. and Gribov, A., (2019). Evaluation of Empirical Bayesian Kriging. *Spatial Statistics*. Vol. 32; 100368. https://doi.org/10.1016/j.spasta.2019.100368

[30]Silva, L. A. and Zanella, G., (2024). Robust Leave-One-Out Cross-Validation for High-Dimensional Bayesian Models. *Journal of the American Statistical Association*. Vol. 119(547); 2369-2381. https://doi.org/10.1080/01621459.2023.2257893

[31]Lumumba, V., Kiprotich, D., Mpaine, M., Makena, N. and Kavita, M., (2024). Comparative Analysis of Cross-Validation Techniques: LOOCV, K-Folds Cross-Validation, and Repeated K-Folds Cross-Validation in Machine Learning Models. *American Journal of Theoretical and Applied Statistics*. Vol. 13(5); 127-137. https://doi.org/10.11648/j.ajtas.20241305.13

[32]Rubinstein, R. Y. and Kroese, D. P., (2016). *Simulation and the Monte Carlo Method*. Wiley. https://doi.org/10.1002/9781118631980

[33]Avcı, H. and Dağ, O., (2024). A Comprehensive Monte Carlo Simulation Study on Multiple Comparison Methods After ANOVA. *Journal of Advanced Research in Natural and Applied Sciences*. https://doi.org/10.28979/jarnas.1429315

[34]Huang, Y., He, Y., Zhu, X. and Chen, Y., (2023). Semi-Analytical Monte Carlo Simulation of Lidar Underwater Target. *Fourteenth International Conference on Information Optics and Photonics (CIOP 2023)*, SPIE p. 105. https://doi.org/10.1117/12.3007528

[35]Driscoll, W., (1996). Robustness of the ANOVA and Tukey-Kramer Statistical Tests. *Computers & Industrial Engineering*. Vol. 31; 265-268. https://doi.org/10.1016/0360-8352(96)00127-1

[36]Rakhmatullaev, S., Marache, A., Huneau, F., Le Coustumer, P., Bakiev, M. and Motelica-Heino, M., (2011). Geostatistical Approach for the Assessment of the Water Reservoir Capacity in Arid Regions: a Case Study of the Akdarya Reservoir, Uzbekistan. *Environmental Earth Sciences*. Vol. 63; 447-460. https://doi.org/10.1007/s12665-010-0711-3

[37]Wheaton, J., Brasington, J., Darby, S. and Sear, D., (2010). Accounting for Uncertainty in DEMs from Repeat Topographic Surveys: Improved Sediment Budgets. *Earth Surface Processes and Landforms*. Vol. 35(2); 136-156. https://doi.org/10.1002/esp.1886

[38]Shiferaw, M. and Abebe, R., (2021). Reservoir Sedimentation and Estimating Dam Storage Capacity Using Bathymetry Survey: a Case Study of Abrajit Dam, Upper Blue Nile Basin, Ethiopia. *Applied Geomatics*. Vol. 13(3); 277-286. https://doi.org/10.1007/s12518-020-00348-x

[39]Khasanov, K. and Bakiev, M., (2026). Assessing Sediment-Induced Storage Capacity Loss in the Hisorak Reservoir, Uzbekistan. *Watershed Ecology and the Environment*. Vol. 8; 23-35. https://doi.org/10.1016/j.wsee.2025.10.004